that can constrain the rotation rate of exoplanets (*22*, *23*) become more valuable and could even be used to constrain their atmospheres.

REFERENCES AND NOTES

1. S. Chapman, R. Lindzen, *Atmospheric Tides, Thermal and Gravitational* (Reidel, Dordrecht, 1970).
2. T. Gold, S. Soter, *Icarus* **11**, 356–366 (1969).
3. A. P. Ingersoll, A. R. Dobrovolskis, *Nature* **275**, 37–38 (1978).
4. A. R. Dobrovolskis, A. P. Ingersoll, *Icarus* **41**, 1–17 (1980).
5. A. C. Correia, J. Laskar, *Nature* **411**, 767–770 (2001).
6. A. C. Correia, J. Laskar, *J. Geophys. Res. Planets* **108** (E11), 5123 (2003).
7. J. F. Kasting, D. P. Whitmire, R. T. Reynolds, *Icarus* **101**, 108–128 (1993).
8. R. Heller, J. Leconte, R. Barnes, *Astron. Astrophys.* **528**, A27 (2011).
9. M. M. Joshi, R. M. Haberle, T. T. Reynolds, *Icarus* **101**, 108–128 (1993).
10. E. S. Kite, E. Gaidos, M. Manga, *Astrophys. J.* **743**, 41 (2011).
11. A. R. Edson, J. F. Kasting, D. Pollard, S. Lee, P. R. Bannon, *Astrobiology* **12**, 562–571 (2012).
12. J. Yang, N. B. Cowan, D. S. Abbot, *Astrophys. J.* **771**, L45 (2013).
13. K. Menou, *Astrophys. J.* **774**, 51 (2013).
14. J. Leconte *et al.*, *Astron. Astrophys.* **554**, A69 (2013).
15. K. Heng, P. Kopparla, *Astrophys. J.* **754**, 60 (2013).
16. A. C. Correia, B. Levrard, J. Laskar, *Astron. Astrophys.* **488**, L63–L66 (2008).
17. D. Cunha, A. C. Correia, J. Laskar, Spin evolution of Earth-sized exoplanets, including atmospheric tides and core-mantle friction. *Int. J. Astrobiol.*, 10.1017/S1473550414000226 (2014).
18. V. V. Makarov, C. Berghea, M. Efroimsky, *Astrophys. J.* **761**, 83 (2012).
19. F. Forget *et al.*, *Icarus* **222**, 81–99 (2013).
20. J. Leconte, F. Forget, B. Charnay, R. Wordsworth, A. Pottier, *Nature* **504**, 268–271 (2013).
21. Materials and methods are available as supplementary materials on *Science* Online.
22. F. Selsis *et al.*, *Astron. Astrophys.* **555**, A51 (2013).
23. I. A. G. Snellen *et al.*, *Nature* **509**, 63–65 (2014).
24. A. C. M. Correia, J. Laskar, O. N. de Surgy, *Icarus* **163**, 1–23 (2003).
25. R. K. Kopparapu *et al.*, *Astrophys. J.* **765**, 131 (2013).

ACKNOWLEDGMENTS

J.L. thanks S. Lebonnois for providing the numerical outputs of the Venus model. The authors thank three anonymous referees for their insightful comments that substantially enhanced the manuscript. N.M. is supported in part by the Canada Research Chair program. This work was supported by grants from the Natural Sciences and Engineering Research Council of Canada to K.M. and N.M. J.L. is a Banting Fellow.

SUPPLEMENTARY MATERIAL

www.sciencemag.org/content/347/6222/632/suppl/DC1
Materials and Methods
Supplementary Text
Figs. S1 to S5
References (*26*–*35*)

14 July 2014; accepted 19 December 2014
10.1126/science.1258686

METALLURGY

Origin of dramatic oxygen solute strengthening effect in titanium

Qian Yu,[1,2]*† Liang Qi,[1]*‡ Tomohito Tsuru,[3] Rachel Traylor,[1] David Rugg,[4] J. W. Morris Jr.,[1] Mark Asta,[1] D. C. Chrzan,[1] Andrew M. Minor[1,2]§

Structural alloys are often strengthened through the addition of solute atoms. However, given that solute atoms interact weakly with the elastic fields of screw dislocations, it has long been accepted that solution hardening is only marginally effective in materials with mobile screw dislocations. By using transmission electron microscopy and nanomechanical characterization, we report that the intense hardening effect of dilute oxygen solutes in pure α-Ti is due to the interaction between oxygen and the core of screw dislocations that mainly glide on prismatic planes. First-principles calculations reveal that distortion of the interstitial sites at the screw dislocation core creates a very strong but short-range repulsion for oxygen that is consistent with experimental observations. These results establish a highly effective mechanism for strengthening by interstitial solutes.

Solutes are intentionally added to pure metals so as to engineer their mechanical properties but may also be present because they are incorporated naturally during processing or service. The strengthening effect of such solutes ordinarily is due to their resistance to dislocation motion, which is conventionally attributed to the elastic interaction between the respective lattice strains of the solute atoms and the dislocations. In isotropic elasticity theory, however, a perfect screw dislocation results in only a shear stress field and does not interact with a solute atom that creates an isotropic volume change (*1*, *2*). The interaction remains relatively weak even when anisotropic elasticity, anisotropic solute strain, and the "modulus effect" of the solute are taken into account. It follows that solution hardening is not ordinarily expected to be an effective hardening mechanism in metals with mobile screw dislocations.

First-principles calculations suggest that under appropriate conditions, there may be a strong, specific structural interaction between solute atoms and the dislocation core that is not captured by the continuum elastic field (*3*, *4*). This raises the possibility that solution hardening may be effective when mobile screw dislocations are present.

The present work addresses solution hardening by small oxygen additions to hexagonally close-packed (HCP) α-Ti. This is a particularly attractive system for such studies both because of its technological importance and because of the dramatic hardening effect of small oxygen additions (*5*–*9*). We exploit recent advances in aberration-corrected transmission electron microscopy (TEM), in situ small-scale mechanical testing, three-dimensional (3D) dislocation analysis, and first-principles computational modeling to clarify solution-hardening in this system. The experimental evidence discussed below documents strong solution-hardening by oxygen, shows substantial solute pinning of screw dislocations, reveals the incorporation of oxygen atoms in the dislocation core, and illustrates interesting features of dislocation motion and reconfiguration in the presence of oxygen. The parallel first-principles calculations clarify the crystallographic source of the oxygen interaction with the screw dislocation core. The distortion of the interstitial sites at the dislocation core creates a very strong but short-range repulsion for oxygen atoms. As a result, dislocations can only move via a "mechanical shuffle" of the oxygen interstitial or by a local cross slip that creates immobile dislocation segments. Both mechanisms effectively pin the dislocation near the oxygen interstitial.

The experimental samples include nominally pure α-Ti with 0.1, 0.2, and 0.3 weight percent (wt %) O additions. All of the materials are solid solutions (their chemical compositions are shown in table S1), although a few precipitates were observed in the Ti-0.3 wt % O sample. Details of the sample preparation are provided in the supplementary materials. In hexagonal α-Ti, the primary mobile dislocations are believed to be <**a**>-type dislocations on the prismatic plane (*1*, *10*), although perpendicular screw dislocations are also active. To characterize dislocations and image the oxygen in their immediate neighborhood, we used the Transmission Electron Aberration-Corrected Microscope (TEAM) 0.5 microscope, a double-aberration-corrected (scanning) TEM capable of producing images with 50-pm resolution (*11*). The types of the dislocations were first determined at low magnification by using standard **g**·**b** analysis. We found that a majority of the "near-edge" dislocations were not pure <**a**>-type; they demonstrated weak contrast under the [0002] reflection, indicating <**c**> components.

[1]Department of Materials Science and Engineering, University of California, Berkeley, CA, USA. [2]National Center for Electron Microscopy, Molecular Foundry, Lawrence Berkeley National Laboratory, Berkeley, CA, USA. [3]Nuclear Science and Engineering Directorate, Japan Atomic Energy, Tokai-mura, Ibaraki, Japan. [4]Rolls Royce, Derby DE24 8BJ, UK.
*These authors contributed equally to this work. †Present Address: Department of Materials Science and Engineering, Zhejiang University, China. ‡Present Address: Department of Materials Science and Engineering, University of Michigan, Ann Arbor, MI, USA.
§Corresponding author. E-mail: aminor@berkeley.edu

Downloaded from http://science.sciencemag.org/ on July 15, 2018

This mixed character was also confirmed through further high-resolution STEM (HR-STEM) studies. Shown in Fig. 1A are typical dark-field and bright-field STEM images of a "near-edge" dislocation core, in which the Burgers circuit in green shows both <**a**> and <**c**> components. The segregation of oxygen atoms at the HCP octahedral sites was observed on the tension side of the edge dislocation core. The atomic structure of edge dislocation cores was similar for both the Ti-0.1 wt % O and Ti-0.3 wt % O samples.

In contrast, the core structures of screw dislocations changed substantially as the oxygen content increased, as illustrated in Fig. 1B. Focusing on screw dislocations with Burgers vector 1/3[11$\bar{2}$0], we plotted the in-plane core atom displacement vectors for the screw dislocation in both Ti-0.1 wt % and Ti-0.3 wt % O samples. We found that the projected view of the screw dislocation core has an extended in-plane displacement field in the Ti-0.1 wt % O sample. However, the screw dislocation core is smaller in projection for the Ti-0.3 wt % O sample, with a narrow displacement field averaging ~0.5 nm in width. Oxygen interstitials are more frequently observed near the core of screw dislocations in the Ti-0.3 wt % O samples, where they occupy octahedral sites, and the displacements are tightly confined to the core, as suggested by the first-principles calculations described in the supplementary materials. The high-resolution TEM observations seem to establish a direct interaction between oxygen interstitials and screw dislocation cores that becomes more apparent as the oxygen concentration increases.

To quantify the impact of such oxygen-dislocation interactions on the mechanical properties, we performed in situ TEM nanocompression tests in which the real-time mechanical response and the evolution of the deformation microstructure were monitored simultaneously. Nanopillars oriented along ⟨01$\bar{1}$0⟩ were prepared from Ti-0.1, Ti-0.2, and Ti-0.3 wt % O bulk polycrystalline samples, respectively, by using focused ion beam milling and Ar^+ cleaning. The pillars were ~150 nm in diameter. Potential Ga damage in the fabrication of the nanopillars was studied (a HR-STEM image of the edge of a nanopillar is shown in fig. S1) and is considered as negligible. These tests isolate the solid solution strengthening effect from any competing influence of precipitation hardening. The dimensions of the pillars are less than the average spacing between oxide precipitates, and the samples were observed to be free of such precipitates. Quantitative nanocompression tests were performed in a JEOL 3010 TEM by using a Hysitron (Eden Prairie, MN) picoindenter in displacement-control mode. The load was applied along the ⟨01$\bar{1}$0⟩ direction. Prismatic slip should be the primary deformation mode in this orientation. The size, orientation, and initial microstructure of the pillars, as well as the structure of the edge dislocation cores, were quite similar across the different samples. Thus, the observed differences in the mechanical properties and deformation microstructure with

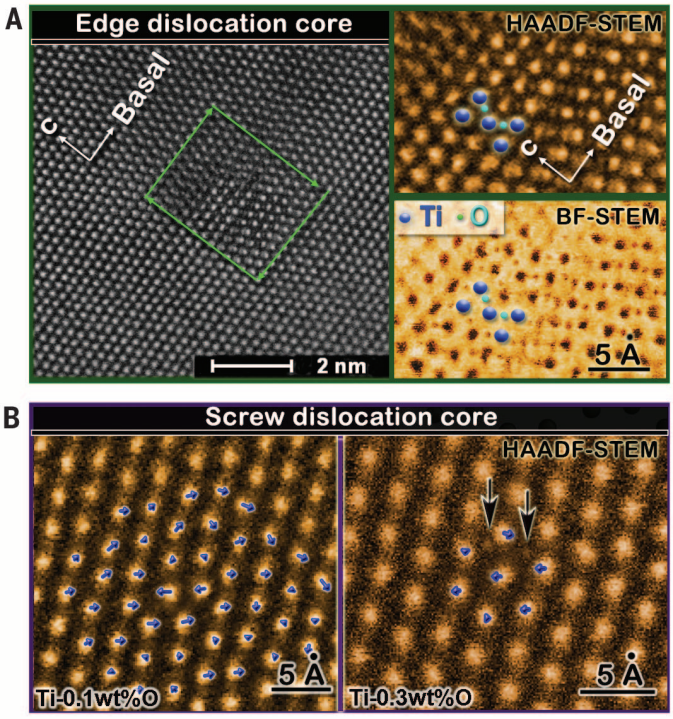

Fig. 1. Imaging of oxygen interstitials and their effect on the dislocation cores in Ti. (**A**) High-angle annular dark-field scanning (HAADF)–STEM image of an edge dislocation core in a Ti-0.1 wt % O sample. Zone axis is [2$\bar{1}\bar{1}$0]. At right are shown higher-magnification HAADF-STEM (top) and the corresponding bright-field STEM image (bottom) of the same edge dislocation core. Oxygen atoms can be seen at the interstitial positions and segregated to the tension side of the dislocation core. (**B**) HAADF-STEM image of a screw dislocation core in Ti-0.1 wt % O (left) and Ti-0.3 wt % O (right). Beam direction is [11$\bar{2}$0]. The in-plane displacement vectors are plotted where each blue vector represents the actual physical displacement of Ti atoms, and the presence of an arrowhead without a tail indicates that the vector is less than or equal to the length of the arrowhead. The blue arrowheads point to the ideal position of the atoms. (Right) The black arrows point to the oxygen atom columns around the screw dislocation core.

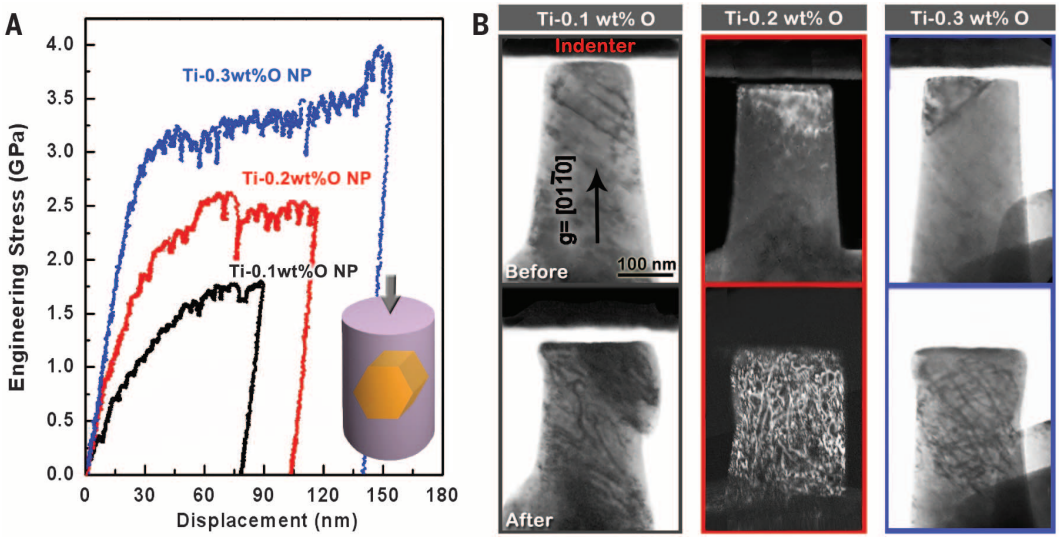

Fig. 2. In situ TEM nanocompression tests of Ti with 0.1, 0.2, and 0.3 wt % O, respectively. (**A**) The engineering-displacement curves of pillar compression tests at different oxygen concentrations. A schematic of the sample and crystallographic orientation is shown bottom right, where the loading direction is along [01$\bar{1}$0]. (**B**) Corresponding TEM images of the pillars before and after compression. *g* vector is along [01$\bar{1}$0]. The Ti-0.1 wt % O and Ti-0.3 wt % O samples were tested under bright-field TEM mode, whereas this Ti-0.2 wt % O sample was tested under dark-field TEM mode.

Downloaded from http://science.sciencemag.org/ on July 15, 2018

increasing oxygen content are expected to be mainly due to the enhanced interaction between the solute atoms and screw dislocations as the concentration increases.

Shown in Fig. 2A are typical engineering stress-displacement curves from nanocompression tests of pillars of varying oxygen concentrations. It is observed that the Ti-0.1 wt % O pillars exhibited the lowest strength, but with substantial work hardening upon yielding. The average yield strength of the Ti-0.3 wt % O pillars was ~2.5 GPa, which is almost 8 times greater than the average yield strength of Ti-0.1 wt % O pillars (~320 MPa). The yield strength of Ti-0.2 wt % O pillars was intermediate between these two samples, as expected. However, the increase in yield strength was not linear with the increase of oxygen concentration. For comparison, bulk compression tests were also performed on these same three alloys at the millimeter scale, with details described in the supplementary materials (fig. S3). It is observed that the oxygen strengthening effect in the nanopillars is stronger than that in bulk samples in which the collective deformation mechanisms are more complex.

As shown in Fig. 2, there were changes in the microstructural deformation pattern as the oxygen content increased. Shown in Fig. 2B are before and after images corresponding to the tests documented in Fig. 2A. As shown in Fig. 2B, most of the pillars contained few preexisting <**a**>-type screw dislocations. After compression, localized primary shear was commonly observed in Ti-0.1 wt % O pillars. Because the pillars were loaded along $\langle 01\bar{1}0 \rangle$, the shear traces can be considered to be associated with prismatic slip. However, as the oxygen concentration increased to 0.2 wt %, localized shear was not typically observed. In the Ti-0.3 wt % O pillars, the plastic deformation was almost homogenous; the pillars eventually deformed into "mushroom" shapes, with no obvious shear localization.

We then matched the in situ TEM movies to the real-time mechanical response of the samples. The results showed that dislocation activity in the Ti-0.1 wt % O pillar shown in Fig. 2B originated from the top of the pillar at about 300 MPa. Localized shear began at ~750 MPa on a prismatic plane that contained one visible preexisting dislocation and continued along this prismatic plane, indicating that the dislocation generation and glide on this plane dominated the deformation. In contrast, pillars with higher oxygen concentrations yielded with a "burst" of dislocations. In the Ti-0.3 wt % O pillar that is shown in Fig. 2B, the stress for the "dislocation-burst" event was ~2.5 GPa, indicating that strong barriers opposed dislocation motion. Moreover, these dislocations were quickly repinned. Eventually, a complex dislocation network developed and filled the volume of the pillar, producing a much more homogenous deformation. These observations are attributable to the increasing oxygen-screw dislocation interaction as the oxygen content was raised.

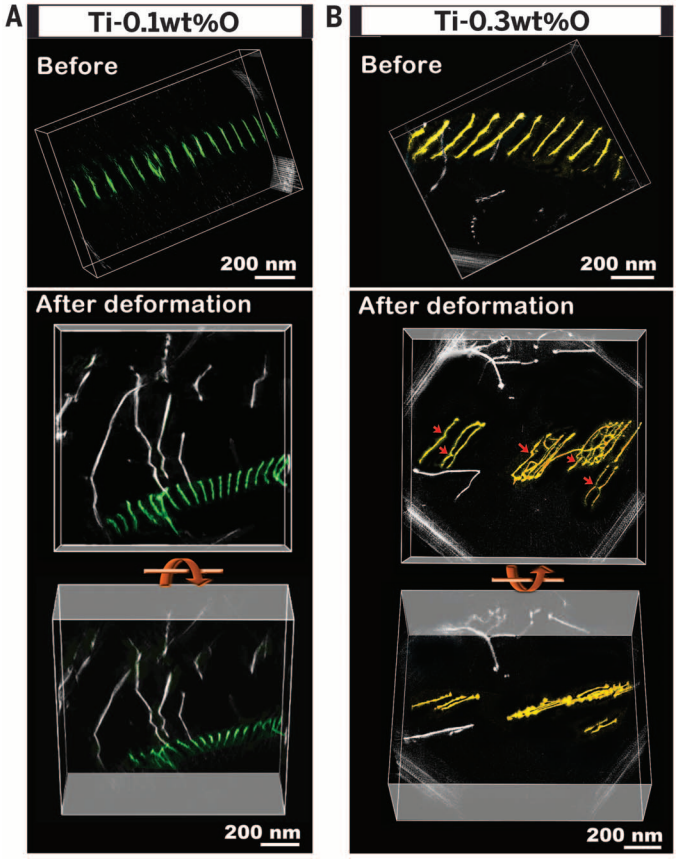

Fig. 3. Tomograms shown the 3D evolution of screw dislocation arrays in Ti-0.1 and Ti-0.3 wt % O, respectively. (**A**) The structure of the dislocation array is similar before and after deformation in Ti-0.1 wt % O. (**B**) The dislocation array has become tangled and moved to different planes after deformation in Ti-0.3 wt % O.

The results from the pillar tests demonstrate that oxygen interstitials act as extraordinarily strong obstacles for the activation of dislocation glide, with the consequence that an addition of only 0.1 wt % O increases the yield stress several times. In addition, the strong pinning effect of oxygen on screw dislocations is reflected in the 3D development of the dislocation deformation microstructure. To investigate the latter phenomenon in more detail, we used a combination of electron tomography and **g·b** analysis to characterize the evolution of screw dislocation arrays. The technique involves the recording of a series of 2D projections of a sample volume at regular intervals over a large angular range, to produce a 3D reconstruction of the sample state. We compared the evolution of screw dislocation arrays that had similar initial configurations and Burgers vectors of $b = \pm[10\bar{1}2]$ in 0.1 and 0.3 wt % O pillars. The tilt series were collected using $g = [10\bar{1}1]$, as detailed in the supplementary materials. Both the Ti-0.1 and Ti-0.3 wt % O samples were then loaded in tension by using a Gatan straining holder ex situ. The samples were loaded to similar displacements, which given the similar sample geometries generates a comparable level of strain. The tilt series were then collected again in the deformed samples, and the changes of the 3D structure of the same dislocation arrays were recorded. Shown in Fig. 3, A and B, are the tomograms of the dislocation arrays before and after strain. After strain, the same location is imaged, and the dislocation arrays found at this location demonstrate that the basic structure of the screw dislocation array was maintained in the Ti-0.1 wt % O samples, whereas some other dislocations, with kinked structures, glided into the nearby region. A tilted view of the original dislocation array shows that the dislocations remained on the same crystal plane. In contrast, the structure of the screw dislocation array (in terms of the average spacing between dislocations and the arrangement of dislocations) was substantially changed during deformation in the Ti-0.3 wt % O samples. In this case, the dislocation array broke up into groups, each containing several dislocation lines with defined pinning points. From the tilted view, it is clear that some groups had slipped onto other crystal planes, promoting the development of a more homogenous deformation pattern. Together, the nanopillar and dislocation tomography experiments demonstrate strong interactions between oxygen interstitials and screw dislocations.

Turning to the theoretical analysis, we began from the observation that solute-dislocation interactions arise from two primary mechanisms: elastic interactions mediated by the long-ranged strain fields produced by a dislocation, and shorter-ranged interactions with the dislocation core that are generally referred to as "chemical" interactions (*4*, *6*). The former are generally weak (on the scale of ~0.1 eV per solute atom); in fact, symmetry constraints have the consequence that there should be no linear elastic interaction at all between oxygen interstitials at octahedral sites and a straight <**a**> screw dislocation in the hcp

Downloaded from http://science.sciencemag.org/ on July 15, 2018

structure (details are provided in fig. S6, and the corresponding analysis is in the supplementary materials). On the other hand, short-range interactions can change the dislocation core structure and influence dislocation mobility by changing the restoring force due to lattice slip. This effect can be described indirectly in terms of the generalized stacking fault (GSF) energy (*12*–*14*)—the energy as a function of the relative displacement of two half crystals parallel to a slip plane—and can be found directly by computing the energetics of the dislocation core structure. Consequently, we used first-principles density functional theory (DFT) calculations (*15*) to find the effects of oxygen interstitial atoms on the GSF energy for slip along the $[11\bar{2}0]$ direction on the Ti prismatic plane and on the core structure of an <**a**> screw dislocation in the Ti lattice.

The calculated results for GSF energy as a function of slip distance are shown in Fig. 4A. Two features of the results are immediately apparent. First, if the O interstitial is located at an octahedral site on the slip plane ("path I"), the calculated GSF energy is much higher than that for pure Ti. Second, as shown in Fig. 4B, the original octahedral site on the slip plane gradually disappears during slip and transforms to a tetrahedral site with much lower interstitial volume when slip is close to 0.5 *a*. At the same time, a new octahedral site is formed on the basal plane of the Ti structure. Transfer of the O atom from the original octahedral site to this newly formed interstitial site reduces the energy by as much as 1.6 eV (fig. S4) (*16*). The GSF energy also can be computed with O at the basal-plane interstitial site ("path II"). As shown in Fig. 4A, this path leads to lower energies than path I once the slip displacement is larger than approximately *a*/4. The barrier for oxygen to shuffle (hop) from the original site in path I to the new site in path II varies from between 0.42 to 0.95 eV, depending on the magnitude of the slip displacement, which is consistent with the large diffusion barrier for oxygen in the bulk hcp Ti structure (*17*). Within the classical Peierls-Nabarro model (*18*), variations in the restoring force on the GSF surface can change the Peierls stress (the minimum stress required to move a straight dislocation at zero temperature) exponentially. The large increase in the GSF energy, coupled with the large barrier (at least 16 times the thermal energy at room temperature) for oxygen shuffle due to lattice slip, qualitatively explains the strong strengthening effects observed in the in situ experiments.

The large changes in GSF energy associated with the presence of oxygen on the slip plane can be correlated with the changes in interstitial volume induced by the slip displacements. These changes are also observed in direct simulations of the core structures of <**a**> screw dislocations in α-Ti, as shown in Fig. 4C. In the bulk hcp structure of Ti, the octahedral site has the largest interstitial volume. Near a screw dislocation core, the interstitial volumes of these octahedral sites decrease by approximately 50% at the geometric center of the dislocation core. On the other hand, a new interstitial site is formed on the basal plane near the core. These changes agree with the change of atomic structure found from the GSF calculations. In addition, the most pronounced changes in the volumes of the interstitial sites are observed on one prismatic plane, on which the core structure of <**a**> screw dislocations in Ti is spread [the spreading of screw dislocation cores on prismatic planes found here is consistent with previous theoretical studies (*19*)].

We also calculated the interaction energies between oxygen interstitial atoms and the dislocation core using DFT. In these calculations, oxygen is inserted into every octahedral site near the dislocation core (details are provided in the supplementary materials), and for each site, the change in energy with respect to placing oxygen far from the dislocation is computed. The results show that the interaction energies are very weak (0.06 eV or smaller) as long as the oxygen is on a prismatic plane other than the one including the dislocation core, or as long as the oxygen is at a distance larger than *c*/2 from the center of the core on the same prismatic plane. The relatively small magnitude of the interaction energies for sites away from the core is consistent with the predictions of the linear theory described above. On the other hand, if oxygen is inserted into the small core region on the same prismatic plane as the dislocation, there is a strong repulsive interaction, which is associated with the small interstitial volume shown in Fig. 4C. In the calculations, this interaction is so strong that the dislocation core is observed to displace from its original position, partially cross slipping onto an adjacent prismatic plane (fig. S5) during the atomic relaxations. In contrast, if the oxygen is inserted into the interstitial site on the Ti basal planes within the core, there is only a small repulsive energy (~0.05 eV), which is consistent with GSF calculations.

The computational results summarized above suggest two effects associated with the interaction of a screw dislocation and oxygen interstitial. First, interstitial oxygen atoms may be forced to move away from their original sites to nearby Ti basal planes because the shear dramatically decreases the volume of the octahedral site. Consistent with this expectation, we have observed by means of HR-STEM oxygen interstitials located on basal planes in some lightly deformed samples (fig. S2); these observations suggest that after the passage of a dislocation, oxygen atoms may become "stuck" in the basal-plane sites rather than hop back to the lower-energy bulk octahedral positions. Second, as shown in Fig. 4D, the presence of oxygen interstitials near the core may force part of the dislocation line to cross-slip to the nearest neighboring prismatic plane. This has the effect of producing two short dislocation edge segments that connect the screw dislocation segments on the two neighboring prismatic planes. These segments can only glide on the basal planes perpendicular to the prismatic planes, and they should thus have very low mobility owing to the larger GSF energy on basal planes (*20*). Additionally, the resolved shear stress for the edge segments is zero under stress conditions that cause motion of the <**a**> screw dislocation along the <**c**> direction on the prismatic

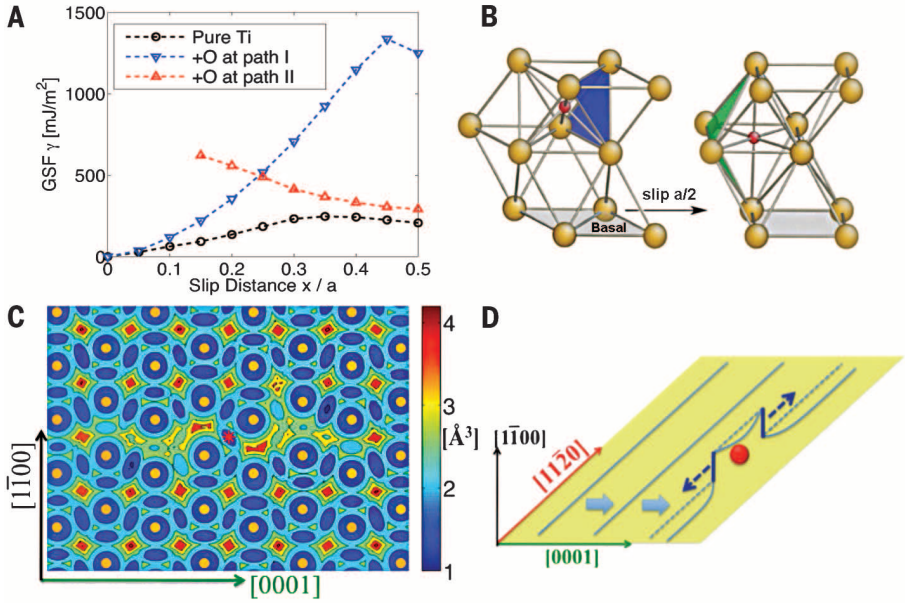

Fig. 4. Simulation results showing the crystallographic source of the oxygen interaction with the screw dislocation core. (**A**) GSF curves for $[11\bar{2}0](1\bar{1}00)$ slip system in ($2a \times 1c$) supercell in Ti with oxygen at different interstitial sites on the slip interface. (**B**) In path I, oxygen is near the original octahedral site in the perfect lattice as the left part figure; in path II, oxygen is at the new octahedral site on Ti basal plane when lattice slip is close to 0.5 *a* (right part). (**C**) Distribution of interstitial volume near <**a**> screw dislocation core. Yellow dots stand for the position of Ti atoms, and the red asterisk in the center is the geometric center of dislocation core. The interstitial volume is defined as $1/6 \times \pi \times d^3$, where *d* is the distance between one point to its nearest Ti atom. (**D**) A schematic of local dislocation cross slip when <**a**> screw dislocation encounters oxygen interstitials.

Downloaded from http://science.sciencemag.org/ on July 15, 2018

plane. The net result is expected to be a pinning of the dislocation core near the oxygen interstitials as shown in Fig. 1B, resulting in strong strengthening effects. The local cross-slipping due to oxygen interstitials is consistent with the tomograms of the dislocation arrays in Ti-0.3 wt % O samples in Fig. 3B. The classical solid solution strengthening model that neglects these two effects may not provide an accurate description of oxygen strengthening in α-Ti (details are provided in the supplementary materials).

The present work establishes a direct connection between the pronounced strengthening effect of oxygen in hcp-structured α-Ti and the strong interactions between these solute atoms with screw dislocation cores. The strongly repulsive solute-dislocation interaction energies, the large barriers for the "mechanical shuffle" of oxygen atoms in the core, and the local cross-slip induced by oxygen interstitials combine to result in a strong pinning effect on screw dislocations. We suggest that these results provide a well-documented, prototypic example of solid solution strengthening by solute interaction with screw dislocations. This type of crystallographically induced strengthening mechanism should also exist for other types of dislocations, depending on the corresponding dislocation core structures and the mobility of solid solute atoms.

REFERENCES AND NOTES

1. J. P. Hirth, J. Lothe, *Theory of Dislocations* (McGraw-Hill, New York, 1982).
2. H. Neuhäuser, *Phys. Scr.* **T49B**, 412–419 (1993).
3. G. P. M. Leyson, W. A. Curtin, L. G. Hector Jr., C. F. Woodward, *Nat. Mater.* **9**, 750–755 (2010).
4. J. A. Yasi, L. G. Hector Jr., D. R. Trinkle, *Acta Mater.* **58**, 5704–5713 (2010).
5. *Metals Handbook* (ASM International, Metals Park, OH, ed. 10, 1990), vol. 2.
6. H. Conrad, *Prog. Mater. Sci.* **26**, 123–403 (1981).
7. G. Lutjering, J. C. Williams, *Titanium* (Springer-Verlag, Berlin, ed. 2, 2007).
8. W. R. Tyson, *Scr. Metall.* **3**, 917–921 (1969).
9. M. L. Wasz, F. R. Brotzen, R. B. McLellan, A. J. Griffin, *Int. Mater. Rev.* **41**, 1–12 (1996).
10. F. D. Rosi, C. A. Dube, B. H. Alexander, *Trans. Am. Inst. Mining Metall. Eng.* **197**, 257 (1953).
11. C. Kisielowski *et al.*, *Microsc. Microanal.* **14**, 469–477 (2008).
12. S. Kibey, J. B. Liu, M. J. Curtis, D. D. Johnson, H. Sehitoglu, *Acta Mater.* **54**, 2991–3001 (2006).
13. G. Lu, N. Kioussis, V. Bulatov, E. Kaxiras, *Phys. Rev. B* **62**, 3099–3108 (2000).
14. V. Vítek, *Philos. Mag.* **18**, 773–786 (1968).
15. G. Kresse, J. Furthmüller, *Phys. Rev. B Condens. Matter* **54**, 11169–11186 (1996).
16. M. Ghazisaeidi, D. R. Trinkle, *Acta Mater.* **76**, 82–86 (2014).
17. H. H. Wu, D. R. Trinkle, *Phys. Rev. Lett.* **107**, 045504 (2011).
18. B. Joós, M. S. Duesbery, *Phys. Rev. Lett.* **78**, 266–269 (1997).
19. M. Ghazisaeidi, D. R. Trinkle, *Acta Mater.* **60**, 1287–1292 (2012).
20. X. Z. Wu, R. Wang, S. F. Wang, *Appl. Surf. Sci.* **256**, 3409–3412 (2010).

ACKNOWLEDGMENTS

We gratefully acknowledge funding from the U.S. Office of Naval Research under grant N00014-12-1-0413. Work at the Molecular Foundry was supported by the Office of Science, Office of Basic Energy Sciences, of the U.S. Department of Energy under contract DE-AC02-05CH11231. T.T. acknowledges the financial support of the Japanese Ministry of Education, Culture, Sports, Science and Technology (MEXT), Grant-in-Aid for Scientific Research in Innovative Areas "Bulk Nanostructured Materials." We thank J. Kacher for dislocation tomography training and Timet (Exton, PA) for the production of the high-purity model alloys used in this study.

SUPPLEMENTARY MATERIALS

www.sciencemag.org/content/347/6222/635/suppl/DC1
Materials and Methods
Supplementary Text
Figs. S1 to S6
Tables S1
References (*21*–*39*)
Movies S1 to S7

27 August 2014; accepted 8 January 2015
10.1126/science.1260485

DNA NANOTECHNOLOGY

Programming colloidal phase transitions with DNA strand displacement

W. Benjamin Rogers[1] and Vinothan N. Manoharan[1,2]*

DNA-grafted nanoparticles have been called "programmable atom-equivalents": Like atoms, they form three-dimensional crystals, but unlike atoms, the particles themselves carry information (the sequences of the grafted strands) that can be used to "program" the equilibrium crystal structures. We show that the programmability of these colloids can be generalized to the full temperature-dependent phase diagram, not just the crystal structures themselves. We add information to the buffer in the form of soluble DNA strands designed to compete with the grafted strands through strand displacement. Using only two displacement reactions, we program phase behavior not found in atomic systems or other DNA-grafted colloids, including arbitrarily wide gas-solid coexistence, reentrant melting, and even reversible transitions between distinct crystal phases.

Like atoms, colloidal particles suspended in a fluid can form bulk phases such as gases and crystals. These particles can also be directed to form new states of matter (*1*) through careful tuning of their interparticle interactions—for example, by grafting DNA strands onto the particles to create specific attractions (*2*, *3*). Such DNA-grafted particles have been called "programmable atom-equivalents" (*4*), a moniker that highlights the experimenter's ability to dictate, or "program," the self-assembled structures through the DNA sequences. The implied analogy to computer programming is a useful way to conceptualize how information in the sequences is translated to structure: Much as one can program a computer to perform complex tasks by writing statements that are compiled to machine code, one can "program" a colloid to form a complex structure by designing nucleotide sequences (statements) that are "compiled" into specific interparticle interactions (machine code). Recent advances in our understanding of this compilation process, in the form of design rules (*5*) or mean-field models (*6*–*8*) relating the effective interactions directly to the nucleotide sequences (*9*), have enabled the assembly of crystal phases not found in ordinary colloids (*5*, *10*–*13*) and could be extended, in principle, to the assembly of prescribed nonperiodic structures (*14*, *15*).

Structure, however, is just one aspect of self-assembly; more generally, self-assembly describes a phase transition between a disordered and an ordered state, or a pathway on a phase diagram. Thus far, only a subset of the full colloidal phase diagram has been programmed: the equilibrium structure of the ordered state as a function of density and composition. Programmatic control over the phase behavior in the orthogonal thermodynamic dimension—the temperature—remains elusive. Typically, the attraction between two DNA-grafted particles decreases steeply and monotonically with increasing temperature (*16*, *17*). As a result, the suspension displays phase behavior resembling that of simple atoms rather than programmable ones: It is fluid at high temperature and solid at low temperature (Fig. 1A). Our goal here is to develop a comprehensive approach to programming the full phase diagram of colloidal suspensions: We seek to design a set of interaction "primitives" that can be combined to program both the structure of equilibrium phases and their temperature-dependent transitions. In other words, we aim to program the equilibrium self-assembly pathways, not just their end points.

We achieve this goal by adding information to the buffer in the form of free DNA strands. We refer to these as displacing strands because their sequences are designed to be complementary to subunits of the grafted strands; they can therefore react with a double-stranded bridge, displacing one of the grafted strands and forming a nonbridging duplex (Fig. 1B). This hybridization reaction, known as toehold exchange or strand displacement, is widely used in the DNA nanotechnology field to construct dynamic assemblies and devices (*18*, *19*). Strand displacement has

[1]School of Engineering and Applied Sciences, Harvard University, Cambridge, MA 02138, USA. [2]Department of Physics, Harvard University, Cambridge, MA 02138, USA.
*Corresponding author. E-mail: vnm@seas.harvard.edu

Downloaded from http://science.sciencemag.org/ on July 15, 2018

Science

Origin of dramatic oxygen solute strengthening effect in titanium

Qian Yu, Liang Qi, Tomohito Tsuru, Rachel Traylor, David Rugg, J. W. Morris Jr., Mark Asta, D. C. Chrzan and Andrew M. Minor

Science **347** (6222), 635-639.
DOI: 10.1126/science.1260485

Screw dislocations: A hard case to crack

The motion of dislocations or defects in a metal influences its strength and toughness. If these defects can be "pinned" by adding alloying elements, it should be possible to create a stronger alloy. It was thought that there shouldn't be much of an interaction between screw dislocations and any alloying elements. However, Yu *et al.* show that for α-Ti, the profound hardening effect of oxygen is due to the strong interactions with the core of the dislocations. First-principles calculations reveal that distortion of the interstitial sites at the dislocation core creates a very strong but short-range repulsion for oxygen atoms.

Science, this issue p. 635

ARTICLE TOOLS http://science.sciencemag.org/content/347/6222/635

SUPPLEMENTARY MATERIALS http://science.sciencemag.org/content/suppl/2015/02/04/347.6222.635.DC1

REFERENCES This article cites 35 articles, 1 of which you can access for free
http://science.sciencemag.org/content/347/6222/635#BIBL

PERMISSIONS http://www.sciencemag.org/help/reprints-and-permissions

Use of this article is subject to the Terms of Service

Science (print ISSN 0036-8075; online ISSN 1095-9203) is published by the American Association for the Advancement of Science, 1200 New York Avenue NW, Washington, DC 20005. 2017 © The Authors, some rights reserved; exclusive licensee American Association for the Advancement of Science. No claim to original U.S. Government Works. The title *Science* is a registered trademark of AAAS.

Downloaded from http://science.sciencemag.org/ on July 15, 2018